Experimental investigation on ferritic stainless steel composite slabs

I. Arrayago*[a], M. Ferrer [b], F. Marimon[b], E. Real[a], E. Mirambell[a]

[a)] *Department of Civil and Environmental Engineering, Universitat Politècnica de Catalunya, Jordi Girona 1-3, Barcelona 08034, Spain*

[b)] *Strength of Materials and Structural Engineering Department, ETSEIB, Universitat Politècnica de Catalunya, Avinguda Diagonal 647, Barcelona 08028, Spain*

Corresponding author: Itsaso Arrayago, itsaso.arrayago@upc.edu, Tel: +34 934054156

ABSTRACT

Steel-concrete composite structures are well established in the construction of floors and roofing, being interesting solutions as steel decks act as formwork for relatively large spans and support the weight of the concrete and construction loads. However, the use of stainless steel decks in such structures has been very limited, although their mechanical properties, corrosion resistance, aesthetics and emissivity make them excellent for visually exposed composite floor slabs where the thermal capacity of the slab is mobilized as part of an energy saving strategy. This paper presents a comprehensive investigation on composite slabs with trapezoidal ferritic stainless steel decks in order to assess the performance of such structural members. Composite slabs made from EN1.4003 ferritic stainless steel and common C25/30 concrete were tested in two series of span lengths in order to determine the different parameters defining their ultimate longitudinal shear response. Reference tests on slabs with galvanized steel were also conducted with identical geometries and configurations. The *m* and *k* parameters used in the *m-k* method and the design longitudinal shear strength $\tau_{u,Rd}$ corresponding to the Partial Connection Method have been determined according to EN 1994-1-1:2004. Finally, the behaviour of these composite slabs was compared with the performance shown by the conducted reference slabs with galvanized steel deck in terms of Ultimate and Serviceability Limit States.

KEYWORDS

composite slab; ferritic stainless steel; *m-k* method; partial connection method; tests

HIGHLIGHTS

- Experimental programme on composite slabs with ferritic stainless steel trapezoidal deck is presented.
- Long span and short span slabs are tested.
- Parameters corresponding to *m-k* and Partial Connection Methods are determined.
- Results are compared to reference tests on galvanized steel for ULS and SLS.

1. INTRODUCTION

The use of deck profiles as steel-concrete composite floor systems and roofing is common in construction, since the steel deck acts as formwork for relatively large spans and supports the weight of the concrete, as well as construction loads. Given that decking profiles usually present unusual shapes and are fabricated from cold-forming procedures, they are characterized by high strength-to-weight ratios, but also by a high susceptibility to buckling. Trapezoidal decks have been employed in building construction since last decades, and the design of such structures is well established in EN 1994-1-1:2004 [1], although the use of stainless steel decks has been very limited since it is a relatively new construction material. The low thermal expansion coefficient and emissivity of ferritic stainless steels allow the mobilization of their thermal capacity in visually exposed composite floor slabs as part of an energy saving strategy, reducing the requirement for heat/cooling in buildings.

Stainless steel is a material with high initial investment requirements, although the consideration of lifecycle costs demonstrate its competitiveness [2]. The absence of nickel in the composition of ferritic stainless steels helps reducing and stabilizing their price, making them especially attractive for construction applications, as established in

[3]. As other stainless steel families, they are characterized by a nonlinear stress-strain behaviour, with a combination of good mechanical and impact properties, excellent corrosion resistance, better response at high temperatures and aesthetics. In recent decades, the use of stainless steel for architectural and construction applications have increased thanks to the research developed on the structural behaviour of stainless steel members and the publication of specific design guidance. The cost of the stainless steel, in relation to that of competing materials, has become much lower, while many new grades and product forms are now widely available all over the world. Nowadays, the stainless steel is not viewed purely as a decorative option for facades and panels and is part of building structures such the roof of the Delhi Parliament Library, the UAE Pavilion at the Shanghaï Expo or the roof in New Doha airport, Qatar as the largest stainless steel roof in the world. There are also some examples for bridges and pedestrian bridges as the Girder Bridge in Stockholm in Sweden, the Cala Galdana Bridge in Menorca (Spain) and the Helix pedestrian bridge in Marina Bay, Singapore [4].

The research has been focussed in the last years in the cross-sectional behavior of I-shaped, circular (CHS), rectangular (RHS) and square hollow sections (SHS) for different types of stainless steels alloys such as austenitic, ferritic and duplex [5-8]. In addition, studies on stainless steel members have been carried out [9-11]. Currently, a new generation of research projects aimed at studying stainless steel structures and the effects of the material non-linearity on the global behavior of frames is active [12-14]. However, the use of ferritic stainless steel decks is not generalized, so the structural performance of such profiles in construction stage and as part of composite slabs needs to be carefully assessed.

This was addressed in the European Research Project entitled Structural Applications in Ferritic Stainless Steel (SAFSS), which provided all the necessary information for the assessment of ferritic stainless steel structural elements. As part of this Research Project, the behaviour of trapezoidal ferritic stainless steel decks as composite floor slabs was investigated (see Figure 1), as reported in Ferrer et al. [15]. First, the structural performance of ferritic stainless steel decks in construction stage was investigated through an extensive experimental programme, where the expressions codified in EN 1993-1-3:2006 [16] and EN 1993-1-4:2006 [17] were assessed. This research was reported by the authors in Arrayago et al. [18], and it was concluded that in general expressions in [16,17] are applicable to ferritic stainless steel decks, although some modified expressions can be used if higher accuracy is required in the design.

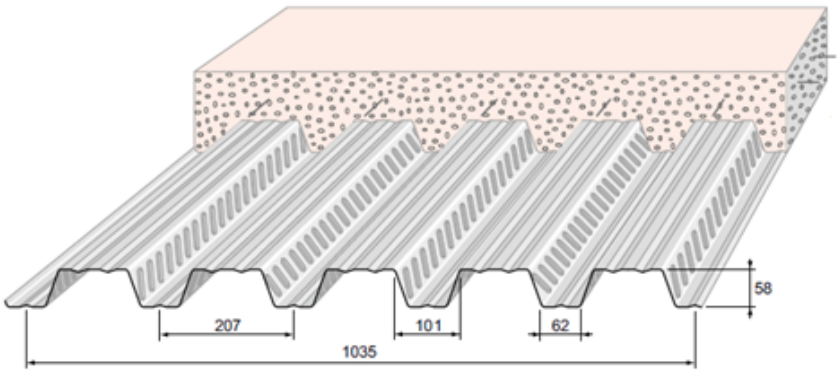

Figure 1 Trapezoidal steel deck in composite floor slab [19]

The behaviour of composite floor slab systems has been systematically investigated during the last decades through different experimental and numerical studies [20-27], and the fire performance of such structures has also been carefully characterized [28-30]. In addition to the punching shear failure, the failure of composite slabs is governed by three major failure modes, as shown in Figure 2, which are bending (for considerably high shear spans L_s), vertical shear (for low shear spans) and longitudinal shear (for intermediate values of L_s), related to the relative slip between the steel deck and the concrete at supports, where the shear span L_s is the distance from the point of

application of concentrated force to its respective reaction force. This paper is focused on this last failure mode, which is the most common for composite slabs, with the purpose of studying the longitudinal shear performance of ferritic stainless steel decks in composite slabs and to determine the values of the different parameters required for the practical use of such decks.

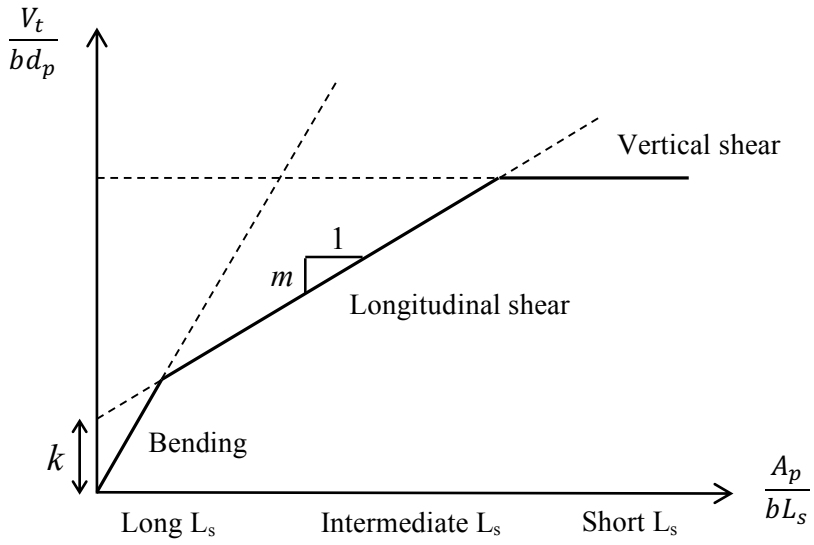

Figure 2 Failures modes for composite slabs, boundaries of the longitudinal shear failure mode

EN 1994-1-1:2004 [1] provides two alternative methods for the design of concrete-steel composite slabs with embossments and without end anchorage: the *m-k* method and the Partial Connection Method (PCM). While the former is applicable to both ductile and brittle slabs, the PCM can only be used for ductile longitudinal shear connections. The longitudinal shear behaviour of composite slabs may be considered as ductile if the failure load exceeds the load causing a recorded end slip of 0,1 mm by more than 10%, according to EN 1994-1-1:2004 § 9.7.3(3) [1]. Both methods require the determination of different parameters which relies on full scale tests, since the complexity of the failure and the parameters affecting the shear bond resistance favoured empirical design methods. Consequently, the obtained parameters are limited to the variables considered in the tests. In order to calculate the *m-k* parameters, slabs with two different shear span

lengths L_s need to be tested, provided that all specimens fail showing longitudinal shear failure modes. Thus, two series of three slabs with intermediate shear spans need to be tested in order to determine the two empirical parameters, m and k. Regarding the PCM, the longitudinal shear strength τ_u (degree of interaction between the deck and the concrete) can be directly derived from the ultimate bending moment resistance of four slab tests showing ductile failure.

This paper presents the experimental programme on composite slabs with ferritic stainless steel decks in order to assess the design provisions for this corrosion resisting material, as well as to obtain the values of the different parameters used in the design of such structures (m-k parameters and the ultimate shear stresses τ_u). Provided that two equivalent specimens with galvanized steel were available, additional tests were carried out on these reference tests for comparison purposes. In addition, obtained results have been compared with similar ferritic stainless steel-concrete composite slabs reported in [31]. These alternative tests consisted on four slabs with different span lengths to those adopted in the present experimental study, which did not allowed for the estimation of the m and k parameters (requiring at least two series of three specimens). Moreover, since the parameters derived from experimental results are limited to the variables considered in the tests, specimens with additional span lengths are of interest.

2. EXPERİMENTAL PROGRAMME

This section describes the conducted experimental programme on composite slabs with ferritic stainless steel trapezoidal decks. The geometry of the slab is first reported, followed by the material properties and pouring procedure. Finally, a comprehensive description of the conducted tests is provided.

2.1 DESCRİPTİON OF THE SLABS

The composite concrete-stainless steel slabs considered in this experimental study comprised a trapezoidal ferritic stainless steel Cofraplus 60 deck and common C25/30 concrete.

2.1.1 Properties of the stainless steel deck

The studied Cofraplus 60 profile is 0.8 mm thick, 58 mm high and presents a total width of 1035 mm, involving 5 waves, according to the requirements in EN 1994-1-1:2004 § B.3.3 (5) [1], which states that the total slab width needs to be wider than three times the overall depth, 600 mm and the cover width of the profiled sheet. The upper part of the waves is reinforced with two stiffeners, while the lower wave shows a single stiffener. Webs are inclined with a 72º angle and present several embossments to guarantee a good connection between the deck and the concrete. These embossments show an inclination of 60º and different direction in both webs for each wave, as shown in Figure 1. A detailed geometrical definition of the representative wave is shown in Figure 3.

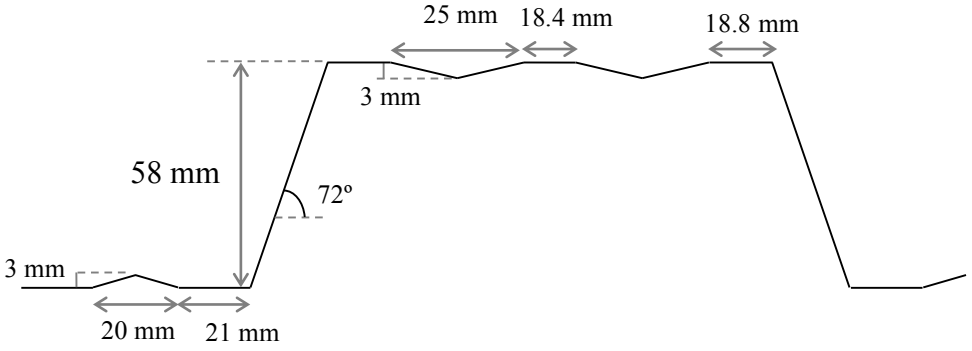

Figure 3 Detailed geometry of a representative wave of the studied deck

In previous investigations by Arrayago et al. [18] the strength of the ferritic stainless steel trapezoidal deck under several loading conditions was investigated. The depth and spacing of the embossments were found to be within the acceptance ranges defined in EN 1994-1-1:2004 § B.3.3 (2) [1], which are 5% and 10% of the nominal values,

respectively. Key geometric and mechanical properties of the studied ferritic stainless steel deck are presented in Figure 4 and summarized in Table 1, in which the design value of the bending moment resistance of the effective cross-section of the profiled steel deck M_{pa} has been adopted as the experimental bending moment resistance in construction stage under positive bending, according to the tests reported in [18].

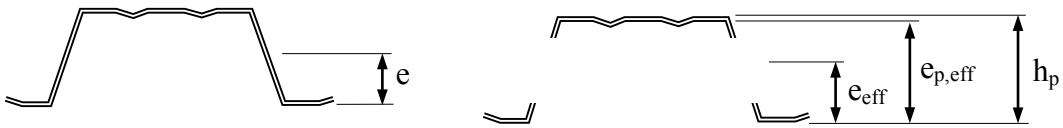

Gross-section Effective cross-section

Figure 4 Definition of key geometric parameters for gross and effective cross-sections

Table 1 Cross-section properties of the ferritic stainless steel deck

Parameter	Value	Description
t	0.8 mm	thickness of the deck
A_p	1211 mm^2	cross-sectional area of the profiled steel deck
A_{pe}	910 mm^2	effective cross-sectional area of the profiled steel deck after removing the embossments
b	1035 mm	total width of the slab
e	32.1 mm	the distance from the centroidal axis of the steel deck to the extreme fibre of the composite slab in tension
e_{eff}	33.3 mm	distance from the centroidal axis of the effective steel deck to the extreme fibre of the composite slab in tension
$e_{p,eff}$	58 mm	distance from the plastic neutral axis of the steel deck to the extreme fibre of the composite slab in tension
M_{pa}	5.7 kNm	design value of the bending moment resistance of the effective cross-section of the profiled steel deck

Material properties of the ferritic stainless steel deck, obtained from tensile coupon tests conducted in [18] are summarized in Table 2, where E is the Young's modulus, $\sigma_{0.2}$ is the proof stress corresponding to a 0.2% plastic strain, conventionally considered as the yield stress (equal to the yield stress f_y for the galvanized steel), σ_u and ε_u are the ultimate strength and strain, respectively, and n and m are the strain hardening exponents. Similar material parameters corresponding to the coupons extracted from galvanized steel decks are also reported.

Table 2 Key material properties of the studied decks

Material	E [MPa]	$\sigma_{0.2}$ [MPa]	σ_u [MPa]	ε_u [%]	n	m
Ferritic stainless steel	218100	326	488	11	12	1.5
Galvanized steel	210000	350	420	16	--	--

2.1.2 Concrete properties and pouring procedure

The concrete used in the tested composite slabs was C25/30 and therefore had a nominal resistance of f_{ck} = 25 N/mm^2. However, and in order to determine the actual resistance of the concrete poured in the slabs, common Ø15cm x 30cm cylindrical specimens were prepared from the same structural concrete delivered for the slabs and had identical curing process as the slabs. These concrete specimens were tested in two sets of four specimens each: the first group was tested right before the first composite slab was conducted, while the second set was tested after the experimental programme was finished. The testing rate was the same for the two sets, 8.85 kN/s, and the results obtained are summarized in Table 3, together with the calculated average strengths f_{cm}.

Table 3 Experimental results from tests on concrete specimens

Test	**Pouring date**	**Test date (48 days/ 106 days)**	**Failure load (kN)**	f_c **(N/mm^2)**
1	10-jan-2013	27-feb-2013	586.6	33.2
2			601.1	34.0
3			597.9	33.8
4			588.0	33.3
			Average strength f_{cm} = 33.6	
1	10-jan-2013	26-apr-2013	679.7	38.5
2			690.9	39.1
3			674.4	38.2
4			705.8	39.9
			Average strength f_{cm} = 38.9	

According to EN 1994-1-1:2004 § B.3.3 (1) [1], decks were used in "as rolled" conditions during slab casting and were not subject to cleaning nor degreasing processes before the concrete was poured, with the aim of not modifying the normal friction and chemical bond conditions. Slabs were fully supported on the ground while the concrete

was poured, since this is the most unfavourable situation for the shear bond mode of failure (see Figure 5(a)), as required in EN 1994-1-1:2004 § B.3.3 (6) [1]. This guaranteed that during the tests the effect of the dead weight of the slab will be totally considered in the measured slips, and the concrete compaction was carried out through an internal needle vibrator, as shown in Figure 5(c). Crack inducers (see Figure 5(a) and (b)) were placed directly under the applied line loads to eliminate the tensile resistance of the concrete. Right after pouring, an electro-welded reinforcing mesh was introduced at a depth of 20 mm from the upper face to avoid any cracking effects due to shrinkage (see Figure 5(d)), which also acted as reinforcement during lifting and transportation against reversal bending moments.

a) General view of the stainless steel deck (long span)

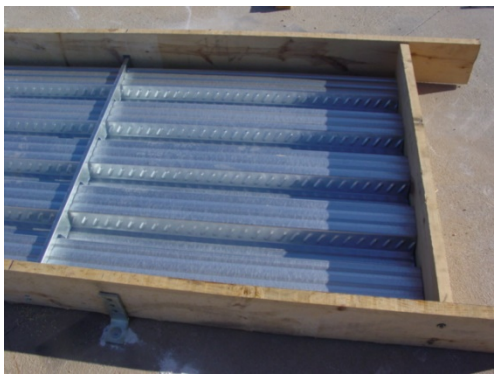

b) Detail of the crack inducer (short span)

c) Concrete compaction using a needle vibrator

d) Superficial reinforcing mesh

Figure 5 Construction of the composite slab specimens

2.2 DESCRIPTION OF THE TESTS

2.2.1 Design of specimens

The experimental programme on ferritic stainless steel composite slabs was carried out following the prescriptions given in EN 1994-1-1:2004, Annex B [1] and consisted of a total of eight composite slab tests. Three long span composite slabs with ferritic stainless steel decks and three with short span were tested, followed by two reference tests on slabs with galvanized steel decks (one for long span and one for short span). Table 4 presents a summary of the conducted tests, where the overall characteristics of the considered slabs are reported. Note that the labelling of the specimen provides information on the deck (C60), the material considered (SS for ferritic stainless steel and CS for galvanized steel), the total length and total height of the specimens, and finally, the number of each test.

Table 4 Summary of the experimental programme on composite slabs

Specimen	Total length [mm]	Span length [mm]	Total height [mm]	Self-weight [kN]	Test type
C60-SS-4400-180-1	4400	4300	180	14.98	static
C60-SS-4400-180-2	4400	4300	180	14.98	cyclic + static
C60-SS-4400-180-3	4400	4300	180	14.98	cyclic + static
C60-CS-4400-180	4400	4300	180	14.98	static
C60-SS-2600-100-1	2600	2500	100	3.95	static
C60-SS-2600-100-2	2600	2500	100	3.95	cyclic + static
C60-SS-2600-100-3	2600	2500	100	3.95	cyclic + static
C60-CS-2600-100	2600	2500	100	3.95	static

2.2.2 Loading scheme

According to EN 1994-1-1:2004, Annex B [1], the test loading procedure is intended to reproduce the loading applied over a period of time and it consists of two different parts. In the initial part, slabs are subjected to cyclic loading, after which the slab is loaded to failure under increasing load. In addition, if two groups of three tests are used, as in this experimental programme, one of the three test specimens of each group should be subjected just to static loading procedure without any cyclic loading in order to

determine the level of the cyclic load for the other two. Therefore, this investigation includes the initial static loading tests on long and short span slabs, which will define the loading procedure to be used in the following cyclic tests.

The cycling loading varies between a minimum value W_{min} not greater than $0.2W_t$ and a maximum value W_{max} not less than $0.6W_t$, according to EN 1994-1-1:2004 § B.3.4(3) [1], where W_t is the maximum total load applied on the slabs, including the measured applied load and the self-weight of the slab and the spread beams, determined from the preliminary static tests. Considering this, and the total loads W_t from the static loading tests, the required limits for the cyclic tests are summarized in Table 5. However, and as it can be observed in this table, the minimum load to be applied to long slabs is lower than the self-weight, which is usual. Due to this fact and other circumstances related to the hydraulic control system (minimum cylinder force around 6.0 kN), the cyclic loadings of the slabs corresponded to those reported in Table 5 for tests. Cyclic loading was applied for 5000 cycles following a sinusoidal signal (0.5 Hz).

Table 5 Summary of limits for cyclic loading in long and short span tests

	Self-weight [kN]	**Load from static test W_t** [kN]	**$0.2W_t$** [kN]	**$0.6W_t$** [kN]	**Min $F_{load\ cell}$** [kN]	**Max $F_{load\ cell}$** [kN]
Long slab **(required)**	15.0	42.3	8.5	25.4	--	9.9
Short slab **(required)**	3.9	39.5	7.9	23.7	3.5	19.3
Long slab **(test)**	15.0	--	22.2	26.5	6.7	10.5
Short slab **(test)**	3.9	--	11.4	23.4	7.0	19.0

The adopted test setups for long and short slabs were defined according to EN 1994-1-1:2004 [1] and are presented in Figures 6 and 7, where the adopted L_{load} and L_s distances were 2150 mm and 1075 mm for long slab tests and 1250 mm and 625 mm for short slabs. The applied load was transmitted to the slabs through two HEB beams and a 100 mm width neoprene pad placed on a sand layer, as shown in Figure 8(b),

which guaranteed a uniformly distributed load. Slabs were simply supported, with boundary conditions consisting of one fixed and one roller supports. This arrangement provides a constant shear force between the point of load application and the point of support, while a pure bending moment loading is achieved at the central span, although the dead weight of the slab slightly modifies these concepts.

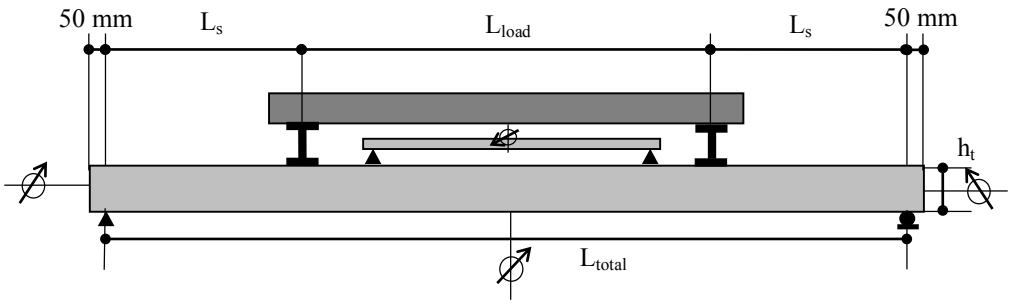

Figure 6 Definition of composite slab tests

Figure 7 General view of the experimental setup for composite slabs

2.2.3 Layout of measurements

Applied loads were measured by means of a load cell and the C60-SS-4400-180-3 specimen was instrumented with strain gauges, which was tested using a reduced cycling loading to produce the expected initial slip and cracking. Slabs were instrumented with several linear displacement transducers measuring deflections at midspan sections, as well as the relative slip of the concrete and the deck at each slab end, as the rotation of the slab end will add difficulty to measure the slip along the slab

axis (as shown in Figure 8(a)). In addition, a final transducer was incorporated to a central curvature measurement device (see Figures 6 and 8(b)-(c)) in order to measure initial cracking of the slab due to pure bending.

a) Detail of the transducer measuring longitudinal slip

b) Uniform load distribution on the sand layer

c) Setup for curvature measurement

Figure 8 Details of the experimental setup for composite slabs

All displacement transducers were set to zero after all test elements were arranged so the effect of the self-weight of the slabs and spreader beams was not included in the measured displacements. In a similar way, the load cell was set to zero while holding the load distribution system so the weight was already included in the load cell output.

3. EXPERİMENTAL RESULTS

This section presents the results of the conducted tests on composite slabs with ferritic stainless steel and galvanized steel decks. Results are summarized in tables for long and short span slabs, and curves showing the load-misdspan deflection and load-longitudinal slip relationships are also reported, as well as figures illustrating the failed slabs. The failure of all tested slabs was clearly due to longitudinal shear, since a very significant relative slip between the deck and the concrete was observed. It is also worth noting that the break of the chemical bond and the first slip occurred early at both sides of the slabs at the very beginning of the first loading ramp for all specimens. Moreover, the significant permanent deflections and slips were completely developed at the first load cycle as well, without any variation in the subsequent 5000 cycles. These

permanent values correspond to the initial slip and deflection values of the response curves showed in next figures.

In order to determine whether each slab showed a ductile or brittle behaviour, the failure loads have been compared to the reference loads causing an end slip of 0.1 mm, as provided in EN 1994-1-1:2004 § 9.7.3(3) [1]. Since the failure loads exceeded the corresponding reference loads by more than the specified 10 %, all tested slabs can be classified as ductile. It should be noted that according to EN 1994-1-1:2004 [1] the failure load of the slab corresponds to the maximum applied load, provided that the midspan deflection is lower than 1/50 of the span length. For long slabs, this limitation had no effect in the definition of the failure load, although for short slabs the restriction lightly affected the maximum load to be considered in this classification. This is explained by the relative slenderness of the studied slabs, given that the height of long slabs was 180 mm while short slabs showed a total height equal to 100 mm.

Experimental results corresponding to long and short span slab tests are reported in Table 6, where the measured loads at 0.1 mm and 0.5 mm slips $F_{0.1mm}$ and $F_{0.5mm}$ are provided in addition to the achieved maximum loads F_u in order to evaluate the ductile behaviour of the slabs and whether the slip needs to be accounted for in the determination of deflections. Midspan displacements δ_u and the longitudinal slips at the failed slab end are also reported. The failure of the long slabs was caused by the slip of one of the ends due to significant cracking of the slabs, as shown in Figure 9.

Table 6 Summary of results for slab tests

Specimen	Load cell Force			Displacements at F_u	
	$F_{0.1mm}$ [kN]	$F_{0.5mm}$ [kN]	F_u [kN]	δ_u [mm]	Slip [mm]
C60-SS-4400-180-1	6.8	6.8	26.9	42.1	6.1
C60-SS-4400-180-2	<10.0	<10.0	29.9	38.9	3.5
C60-SS-4400-180-3	5.0	6.9	32.6	43.5	7.1
C60-CS-4400-180	25.4	25.4	31.6	31.7	4.4
C60-SS-2600-100-1	3.6	9.8	34.5	35.1	52.6
C60-SS-2600-100-2	3.5	9.9	36.7	39.5	70.7
C60-SS-2600-100-3	4.4	7.9	34.9	36.2	66.8
C60-CS-2600-100	23.5	20.0	34.2	36.1	75.2

Figure 9 Long slabs after slip failure

The load-deflection curves measured in the long slabs are presented in Figure 10, where the average deflections of the midspan section are plotted, whereas Figure 11 shows the load-longitudinal slip curves for the same specimens. In both figures, cyclic residual deflections and slips have been included. The different performance of ferritic stainless steel and galvanized steel slabs is worth mentioning, although the detailed analysis is given in Section 4. As it can be appreciated in these figures, the initial slip of cycled specimens (#2 and #3) are similar for both slab lengths (below 2 mm, see Figures 11 and 14), although the relative dispersion is higher in the case of long slabs than for the short ones. Note that this higher slip dispersion in long slabs is magnified in terms of mid-span deflections (Figure 10).

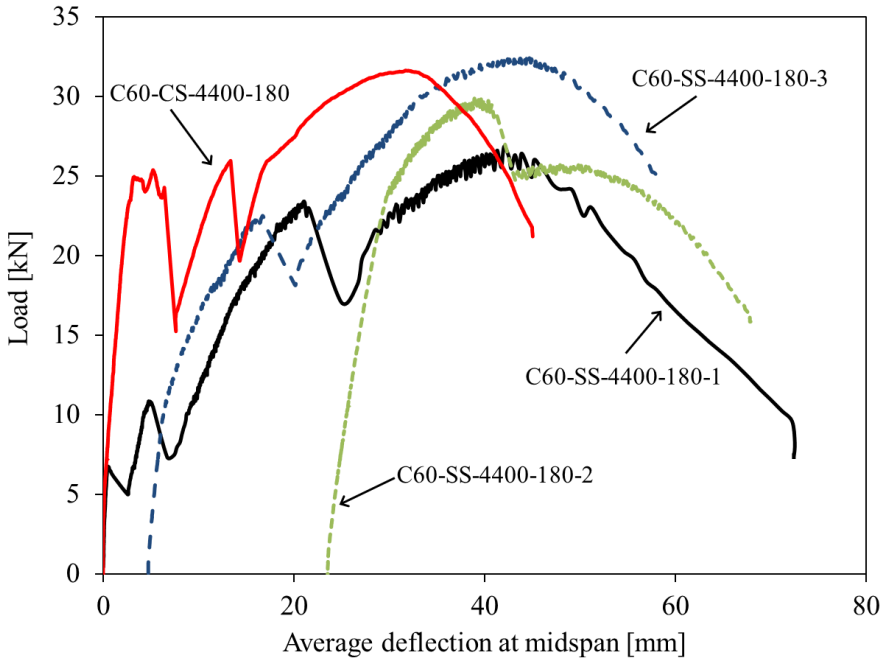

Figure 10 Load-midspan deflection curves for long span slab tests (cycling residual deflections included)

1

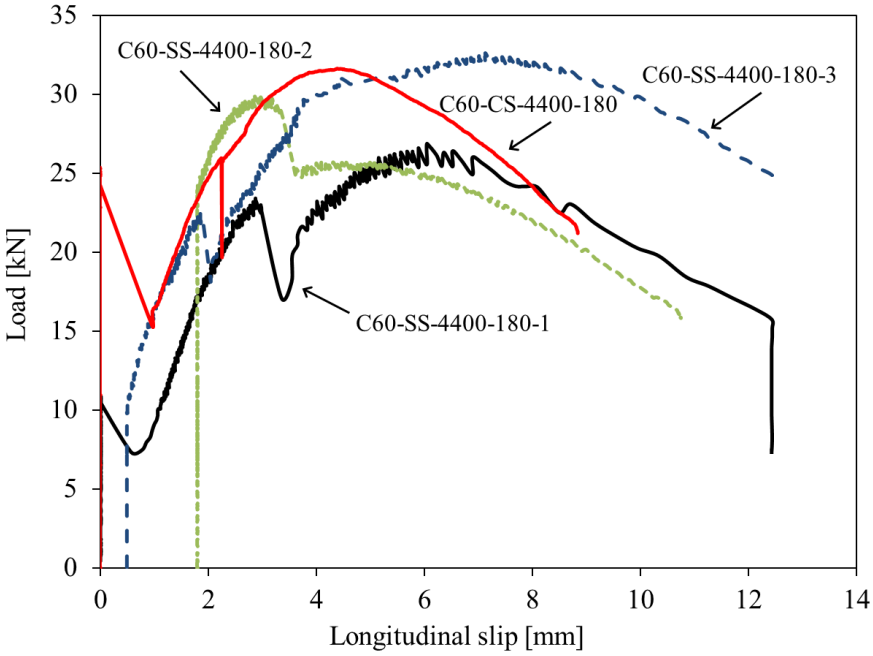

Figure 11 Load-slip curves for long span slab tests (cycling residual deflections included)

2 Figure 12 shows one of the short slabs after longitudinal shear failure, while the load-
3 deflection curves corresponding to the tested short slabs are presented in Figure 13 and
4 the load-longitudinal slip curves are shown in Figure 14 for the same specimens.

1

Figure 12 Short slab after longitudinal shear failure

2

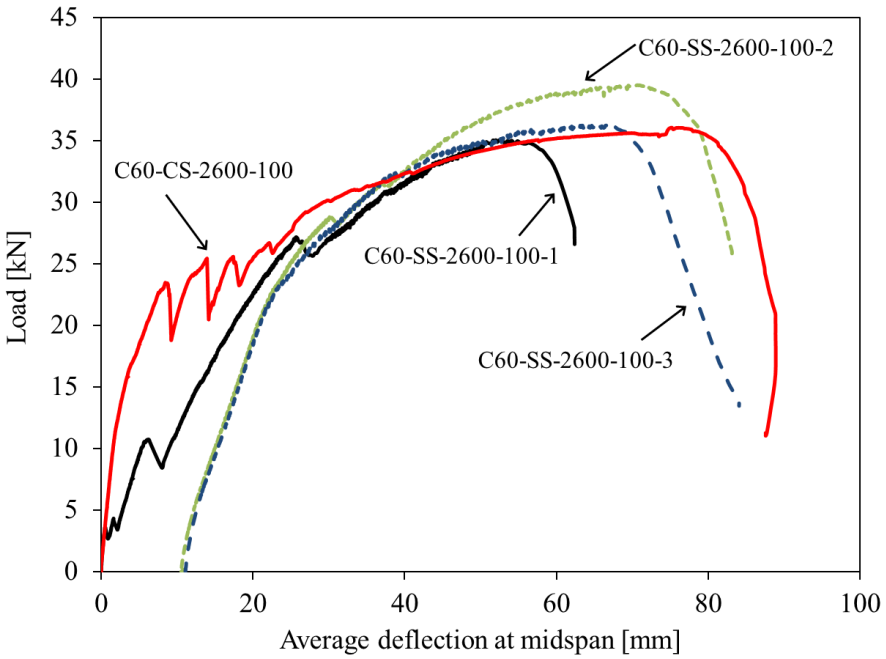

Figure 13 Load-midspan deflection curves for short span slab tests (cycling residual deflections included)

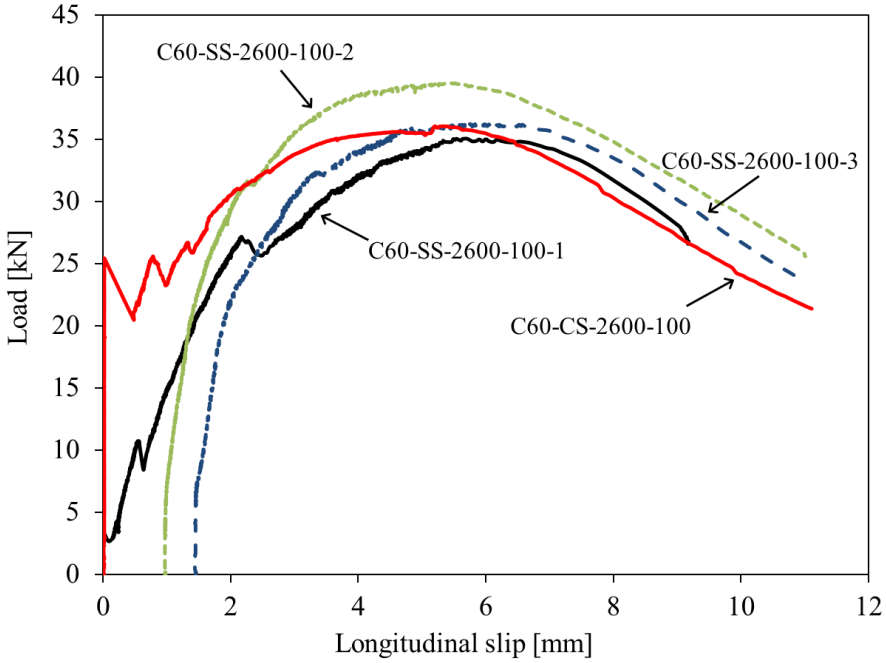

Figure 14 Load-slip curves for short span slab tests (cycling residual deflections included)

As mentioned before, the objective of conducting a preliminary cyclic loading in composite slabs is to eliminate the chemical bond between the steed deck and the concrete. As no noticeable differences are observed in reached ultimate loads (the ultimate load corresponding to cycled specimens are even higher sometimes) it can be highlighted that the ultimate loads do not depend on the initial chemical bond. Moreover, in this case, the chemical bond between the stainless steel deck and the concrete is very low or even inexistent. This will be investigated and commented more in detail in the following sections, to evaluate the influence of the chemical composition of the steel and the superficial roughness in this chemical bond.

4. ANALYSİS OF EXPERİMENTAL RESULTS

Results obtained from the conducted experimental programme on ferritic stainless steel composite slabs can be used to determine the design parameters according to EN 1994-1-1:2004 [1], which will allow similar composite slabs to be designed in the future. Since all slabs failed due to longitudinal shear, the two methodologies included

in EN 1994-1-1:2004 [1] for this failure mode have been investigated in this section, the *m-k* Method and the Partial Connection Method.

4.1 THE *m-k* METHOD

The *m-k* Method is a semi-empiric design method for composite slabs with embossments based on the assumption that the ultimate shear force is linearly dependent on $1/L_s$, where L_s is the shear span length, in which the shear resistance is determined by means of slab tests. Thus, for the estimation of the m and k parameters defining the longitudinal shear failure mode, two groups of slabs showing different shear span lengths are required. In this method, the design shear resistance $V_{l,Rd}$ given in Eq. (1) is determined from the m and k parameters, as shown in Figure 2. In this expression, b and L_s are the slab width and shear span length of the slab, d_p is the distance between the centroidal axis of the profiled steel deck and the extreme fibre of the composite slab in compression, A_p is the cross-sectional area of profiled steel deck and γ_{VS} is the partial factor for design shear resistance of a composite slab.

$$\mathrm{V_{Ed}} \leq \mathrm{V}_{l,Rd} = \frac{b d_p \left(\frac{m A_p}{b L_s} + k\right)}{\gamma_{VS}} \tag{1}$$

For the determination of the m and k parameters, both long and short span slabs have been considered and experimental results have been plotted in the $V_t/(b \cdot d_p) - A_p/(b \cdot L_s)$ diagram, as shown in Figure 15. Support reactions V_t have been calculated as $V_t = W_t/2$ and since all specimens showed a ductile behaviour, no reduction was applied. According to EN 1994-1-1:2004 § 9.7.3 and B.3.5 [1], the m and k parameters defining the longitudinal shear failure can be estimated from the experimental results provided that the deviation of these results is less than 10% of the average value, which Tables 6 proofs to be satisfied. Thus, the characteristic values of each slab group are obtained by reducing in a 10% the corresponding lowest value,

resulting in m = 134 N/mm^2 and k = –0.0329 N/mm^2, as represented in Figure 15. It should be pointed that such negative k values are commonly obtained in some cases, typically in open-rib profiles or when lightweight concrete is used [32].

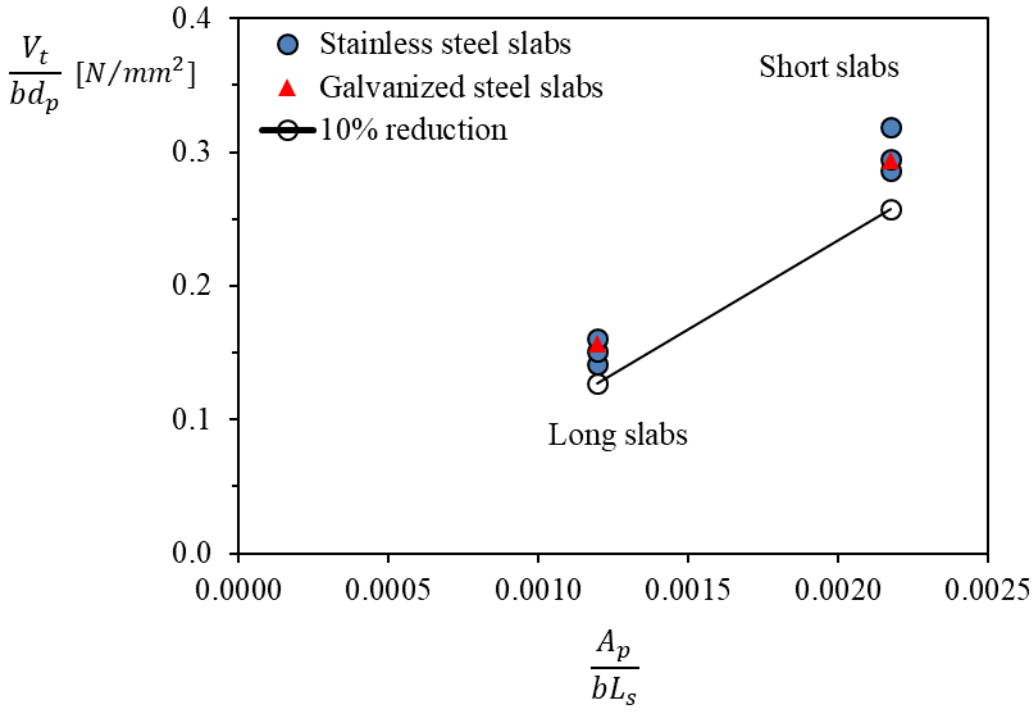

Figure 15 Linear interpolation defining the longitudinal shear failure mode for ferritic stainless steel specimens

4.2 THE PARTIAL CONNECTION METHOD

The Partial Connection Method determines the degree of connection corresponding to each of the tested composite slabs, which ranges between the two extreme situations, the full connection (η=1) where the plastic bending moment of the composite section is reached, and the situation with no connection (η=0), where only the plastic efficient bending moment of the steel deck is considered. Between these limits, EN 1994-1-1:2004 [1] considers an interpolation model assuming that in partial interaction the slip behaviour is ductile enough to let both materials reach their ultimate capacity.

The degree of shear connection η is defined as the ratio between the concrete compression force at partial connection N_c and at full connection $N_{c,f}$, as given in

Eq. (2), where $f_{yp,d}$ is the design value of the yield strength of the profiled steel deck, $\tau_{u,Rd}$ is the design value of the longitudinal shear strength and L_x is the distance from a cross-section to the nearest support. The stress diagram of the composite section corresponding to the partial connection ultimate limit state is presented in Figure 16.

$$\eta = \frac{N_{\mathrm{c}}}{N_{\mathrm{c,f}}} = \frac{N_{\mathrm{c}}}{A_{\mathrm{pe}} f_{\mathrm{yp,d}}} = \frac{\tau_{\mathrm{u,Rd}} b L_x}{A_{\mathrm{pe}} f_{\mathrm{yp,d}}} \tag{2}$$

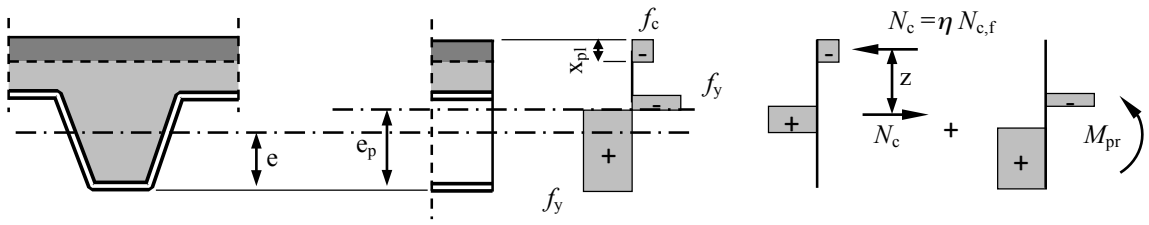

Figure 16 Stress distribution in sagging bending in partial connection

According to EN1994-1-1:2004 [1], the design bending moment resistance M_{Rd} is given by Eq. (3), where z is the lever arm for N_c according to Eq. (4) and M_{pr} is the reduced plastic resistance moment of the profiled steel deck, as for Eq. (5).

$$M_{\mathrm{Ed}} \le M_{\mathrm{Rd}} = N_c \cdot \mathrm{z} + M_{\mathrm{pr}} = \tau_{\mathrm{u,Rd}} b L_x \cdot \mathrm{z} + M_{\mathrm{pr}} \tag{3}$$

$$\mathrm{z} = h - 0{,}5 x_{\mathrm{pl}} - e_{\mathrm{p}} + \left(e_{\mathrm{p}} - e\right)\eta \tag{4}$$

$$M_{\mathrm{pr}} = 1{,}25 \cdot M_{\mathrm{pa}}(1 - \eta) \le M_{\mathrm{pa}} \tag{5}$$

The design value of the shear resistance $\tau_{u,Rd}$ can be determined from a series of three composite slab tests and slabs of one single span are sufficient according to EN 1994-1-1:2004 [1]. However, EN 1994-1-1:2004 [1] establishes that the span length should be as long as possible, provided that the slab will fail due to longitudinal shear. Although the short span slab tests are not necessary for the determination of the shear resistance $\tau_{u,Rd}$, and provided that they showed longitudinal shear failure modes, an additional value of $\tau_{u,Rd}$ has been calculated for comparison purposes.

From the equations listed above and considering the measured mean strength values for the ferritic stainless steel decks and concrete, the partial interaction diagram of the studied slabs can be derived. According to EN 1994-1-1:2004 § B.3.6 (2) and (3) [1], the partial connection degree η and the ultimate shear stresses $\tau_{u,Rd}$ can be then obtained from the measured ultimate bending moment of each test, as for Eq. (6), L_0 is the length of overhang (L_0=50 mm), μ is the default value of friction coefficient (if taken into account, the recommended value is μ=0.5) and V_t is the reaction at the support. The partial connection degree η can be directly calculated by solving the quadratic equation given in Eq. (7) and once τ_u values are determined, the characteristic $\tau_{u,Rk}$ and the design values $\tau_{u,Rd}$ can be easily derived.

$$\tau_{\mathrm{u}} = \frac{\eta N_{\mathrm{c,f}} - \mu V_{\mathrm{t}}}{b(L_{\mathrm{x}} + L_0)} \tag{6}$$

$$M_{\mathrm{u,test}} = \eta N_{\mathrm{c,f}} \cdot \left(h - 0{,}5\eta x_{\mathrm{pl,f}} - e_{\mathrm{p}} + \left(e_{\mathrm{p}} - e\right)\eta\right) + 1{,}25M_{\mathrm{pa}}(1-\eta) \tag{7}$$

From the equations presented above and for the ultimate bending moments corresponding to the failure loads of the ferritic stainless steel composite slab tests, the following ultimate shear stresses $\tau_{u,Rd}$ can be derived. In this study, the M_{pa} value obtained from the previous experimental programme on ferritic stainless steel decks in construction stage by Arrayago et al. [18] has been considered. Results accounting for the additional longitudinal shear resistance caused by the support reactions are presented in Table 7, together with those corresponding to the ultimate shear stresses without considering the effect of the support reaction. The characteristic shear strengths $\tau_{u,Rk}$ have been calculated from the test values as the 5% fractiles using an appropriate statistical model in accordance with EN 1990:2005, Annex D [33], and the design strengths $\tau_{u,Rd}$ have been then obtained as the characteristic strengths divided by the γ_{VS}

partial safety factor (γ_{VS} =1.25 as recommended in EN 1994-1-1:2004 [1]). Results in Table 7 indicate that the derived ultimate shear stresses are very similar for ferritic stainless steel and galvanized steel decks, showing an equivalent response at failure.

These values are also comparable to those reported by Lauwens et al. [31] for tests on composite slabs with ferritic stainless steel trapezoidal decks. For this experimental programme the same Cofraplus60 cross-section made from ferritic stainless steel grade EN1.4003 was considered, although the tested span lengths and total slab heights were slightly different. All slabs reported in [31] were 100 mm high, and while three tests were conducted for a span length of 1800 mm, a single slab was tested with a 1300 mm span length. For the short specimen a design ultimate shear stress $\tau_{u,Rd}$ accounting for the effect of the support reaction equal to 0.293 N/mm^2 was derived, while for the long specimens $\tau_{u,Rd}$ was 0.194 N/mm^2 in [31]. This last design ultimate shear stress is comparable to that obtained for the short specimens in the present experimental programme, 0.167 N/mm^2, since the adopted slab height are the same, with considerably similar span lengths. Calculated shear stress values are similar, being those corresponding to slabs with L = 2600 mm lower since they are longer than those reported in [31].

Table 7 Longitudinal shear resistance of composite slabs with ferritic stainless steel decks

	Specimen	$M_{u,test}$ [kNm]	$\eta=N_c/N_{c,f}$	Accounting for the effect of the support reaction			Without accounting for the effect of the support reaction		
				τ_u [N/mm^2]	$\tau_{u,Rk}$ [N/mm^2]	$\tau_{u,Rd}$ [N/mm^2]	τ_u [N/mm^2]	$\tau_{u,Rk}$ [N/mm^2]	$\tau_{u,Rd}$ [N/mm^2]
Long slabs	C60-SS-4400-180-1	21.16	0.442	0.113			0.123		
	C60-SS-4400-180-2	22.65	0.485	0.125	0.114	**0.092**	0.135	0.124	**0.100**
	C60-SS-4400-180-3	24.03	0.524	0.135			0.146		
	C60-CS-4400-180	23.54	0.506	0.133	0.133	0.106	0.144	0.144	0.115
Short slabs	C60-SS-2600-100-1	10.85	0.459	0.208			0.224		
	C60-SS-2600-100-1	12.08	0.565	0.258	0.209	**0.167**	0.276	0.225	**0.180**
	C60-SS-2600-100-1	11.18	0.488	0.222			0.238		
	C60-CS-2600-100	11.13	0.494	0.229	0.229	0.183	0.246	0.246	0.197

4.3 COMPARISON OF STAINLESS STEEL AND GALVANIZED STEEL SLABS

From the comparison of the experimental results for ferritic stainless steel and galvanized steel composite slabs, it can be seen that differences on the ultimate loads are not appreciable. Thus, differences between the parameters governing the Ultimate Limit State (ULS) are not significant regardless the considered design method. Both the *m-k* Method and the Partial Connection Method provide similar results when applied to slabs with ferritic stainless steel or galvanized steel decks.

However, from the comparison of the results corresponding to slabs with ferritic stainless steel and galvanized steel decks in Figures 11-14 it can be concluded that stainless steel decks show a considerably lower resistance to first slip (>0.1 mm) than slabs with conventional galvanized steel. The weaker initial adherence is attributed to the much smoother surface of the stainless steel deck and also to the different chemical reactions between the concrete and stainless steel or zinc surfaces. Regarding the Serviceability Limit State (SLS), the low resistances corresponding to the 0.5 mm slips (see $F_{0.5mm}$ values in Table 6) exhibited by ferritic stainless steel decks might make necessary to provide end anchors or to consider the slip effect when calculating deflections under service loads, as established in EN 1994-1-1:2004 § 9.8.2(7) [1]. Other design provisions, such as the French National Annex, NF EN1994-1-1/NA by Commission de normalisation de la construction mixte CNCMIX [34] and the technical advice for composite slabs in Commission chargée de formuler des Avis Techniques [35], are even more restrictive in terms of Serviceability Limit State and limit the first slip of slabs to 0.1 mm.

Ertzibengoa et al. [36] studied the influence of the material and its roughness in the steel-concrete bond by conducting several push-out tests on carbon steel and two different grades of austenitic and ferritic stainless steel rebars. In [36], the authors

concluded that the factors affecting the concrete-steel adhesion behaviour are the geometry, the material type and the micro-roughness (R_a). According to [36], the influence of the material on the developed bond capacity is more relevant for smooth samples (without any rib or macroscopic roughness) than for ribbed ones, since the bond behaviour in smooth samples is primarily governed by the chemical adhesion mechanism. It was observed that the bond strength can be around 85% higher in carbon steel than in austenitic stainless steel due to the different material type, while the ferritic grade showed a much lower bond strength. The authors in [36] also studied the influence of the roughness in the bond strength by analysing the same austenitic stainless steel grade with two different surface finishes. The study concluded that a R_a variation from 3 μm to 0.4 μm results in a 20% bond strength reduction. Considering that the tested specimens involved galvanized steel and ferritic stainless steel decks, the different behaviour of the slabs obtained in this present study is consistent with the results published by [36]. With the aim of measuring these effects, this paper presents an additional study on the deck-concrete bond. The experimental results presented in the previous sections highlighted the different bond strength of galvanized and stainless steel decks with identical geometries.

Roughness tests were performed by the deck producer in galvanized and ferritic stainless steel specimens. Five roughness measurements were carried out for each material type, providing mean R_a micro-roughness values of 0.76 μm for galvanized steel specimens and 0.03 μm for ferritic stainless steel samples. Examples of typical roughness measurements for galvanized and stainless steel specimens are shown in Figure 17. As these figures show, the roughness of the galvanized specimen is about 25 times higher than for ferritic stainless steel, which, together with the different material composition, explains the different behaviour in initial slip of the slabs. Nevertheless,

the particular influence of the material type and roughness could not be determined since galvanized steel decks with micro-roughness similar to that shown by the tested stainless steel decks were not available to test.

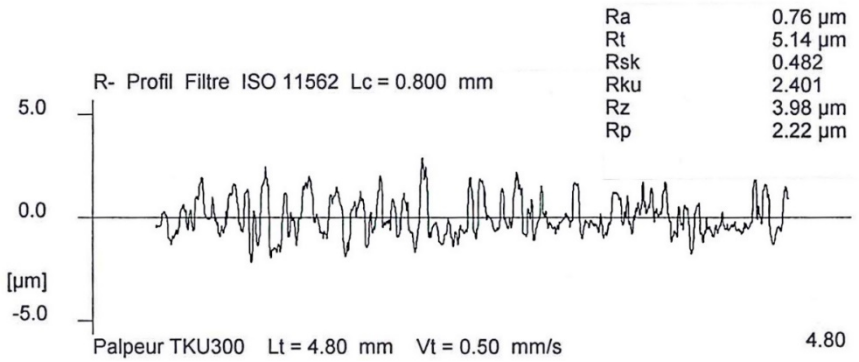

a) In galvanized steel specimen

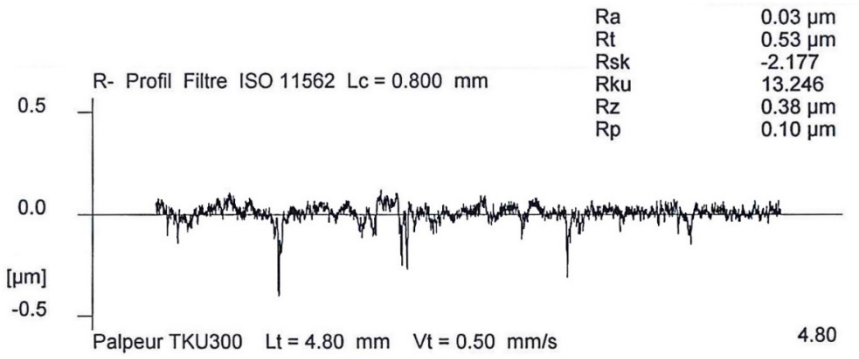

b) In ferritic stainless steel specimen

Figure 17 Roughness measurements

However, if stainless steel decks with higher roughness were used for composite slab construction, the need of end anchors or the consideration of the effect of the slip in the calculation of deflections could be avoided according to the conclusions in [36]. Hereafter, it is important to ensure that the side of the stainless steel deck which will be in contact with concrete has the appropriate roughness in order to avoid a premature split of the slab. The roughness of the deck surface can be improved by several methods such as bead and shot-blasting by the impact of a hard and inert material (e.g. glass, ceramic, stainless steel shot among others), which provides enhanced surface properties similar to those obtained by acid etching. If a special finish of the deck is needed for

visually exposed construction, this can be solved by providing the required surface finish just to the exposed side of the deck.

5. CONCLUSIONS

This paper presents a comprehensive experimental investigation on eight composite slabs under simply supported conditions with trapezoidal ferritic stainless steel Cofraplus 60 decks, where the behaviour of the specimens in Ultimate and Serviceability Limit States (ULS and SLS) has been studied. The study considered in this paper focused on the longitudinal shear failure mode, characterized by the relative slip between the steel deck and the concrete at supports and which is the most common for composite slabs.

The different parameters defining the ultimate longitudinal shear response according to the two design methods provided in EN 1994-1-1: 2004 [1] have been determined from the full scale tests:

- The m and k parameters for ferritic stainless steel decks equal to m = 134 N/mm^2 and k = –0.0329 N/mm^2 were obtained.

- Regarding the Partial Connection Method, the longitudinal shear design strengths $\tau_{u,Rd}$ with and without considering the effect of the support reactions have been determined, which corresponded to 0.092 N/mm^2 and 0.100 N/mm^2 respectively.

The behaviour of composite slabs with ferritic stainless steel decks was compared to the performance shown by the reference slabs with galvanized steel deck in terms of ULS and SLS. Experimental results demonstrated that differences on the ultimate loads and parameters governing the ULS are not significant. However, slabs with ferritic stainless steel decks exhibited an early first slip, which was attributed, according to [36], to the different chemical reactions between the concrete and stainless steel and to the considerably lower superficial micro-roughness.

The low resistances corresponding to the 0.5 mm slips at SLS shown by ferritic stainless steel decks might make necessary end anchors or the consideration of the slip effect in the calculation of deflections under service loads, as established in [1]. Nevertheless, this could be avoided if decks showing higher and appropriate roughness at the side in contact with concrete were used for composite slab construction to dodge a premature split of the slab (by means of bead or shot-blasting). For visually exposed slabs, the required surface finish could be provided to the exposed side of the deck.

ACKNOWLEDGMENTS

The research leading to these results has received funding from the European Community's Research Fund for Coal and Steel (RFCS) under Grant Agreement No. RFSR-CT-2010-00026, as well as from the Ministerio de Ciencia e Innovación (Spain) under the Project BIA2010-11876-E "Acciones complementarias".

REFERENCES

[1] EN 1994-1-1, European Committee for Standardization (2004), "Eurocode 4. Design of composite steel and concrete structures. Part 1-1: General rules and rules for buildings", Brussels, Belgium.

[2] Baddoo, N.R. (2008), "Stainless steel in construction: a review of research, applications, challenges and opportunities", *Journal of Constructional Steel Research*, **64**(11), 1199-1206.

[3] Cashell, K.A. and Baddoo, N.R. (2014), "Ferritic stainless steels in structural applications", *Thin-Walled Structures*, **83**, 169–181.

[4] Baddoo, N.R. (2013), "Steel Appeal", *The Structural Engineer*, **91**(8), 9–18.

[5] Afshan S. and Gardner L. (2013). "Experimental study of cold-formed ferritic stainless steel hollow sections". *Journal of Structural Engineering (ASCE),* **139**(5), 717-728.

[6] Bock M., Arrayago I. and Real E. (2015). "Experiments on cold-formed ferritic stainless steel slender sections". *Journal of Constructional Steel Research*, **109**, 13–23.

[7] Lecce M. and Rasmussen K.J.R. (2006). "Distortional buckling of cold-formed stainless steel sections: experimental investigation". *Journal of Structural Engineering (ASCE)*, **132**(4), 497–504.

[8] Buchanan C., Real E. and Gardner L. (2018). "Testing, simulation and design of cold-formed stainless steel CHS columns". *Thin-Walled Structures*, **130**, Pages 297-312.

[9] Arrayago I., Real E. and Mirambell E. (2016). "Experimental study on ferritic stainless steel RHS and SHS beam-columns". *Thin-Walled Structures*, **100**, 93–104.

[10] Huang Y. and Young B. (2013). "Tests of pin-ended cold-formed lean duplex stainless steel columns". *Journal of Constructional Steel Research*, **82**, 203–215.

[11] Afshan S., Zhao O. and Gardner L. (2017). "Buckling curves for stainless steel tubular columns". *Proceedings of Eurosteel 2017*, **1** (2-3), 3481-3490.

[12] Di Sarno L., Elnashai A.S., Nethercot D.A. (2005). "Seismic response and design of stainless steel frames". *Proceedings of the Fourth International Conference on Advances in Steel Structures* 13–15, 1253–1258. Shanghai, China.

[13] Arrayago I., Real E., Mirambell E., Chacón R. "Global plastic design of stainless steel frames". *Proceedings of Eurosteel* 2017, **1** (2-3), 3463-3471.

[14] Walport F., Nethercot D., Real E., Arrayago I., Gardner L. (2018). Effects of material nonlinearity on the global analysis of stainless steel frames. *Journal of Constructional Steel Research*. *In press*

[15] Ferrer, M., Marimon, F., Arrayago, I., Real, E. and Mirambell, E. (2013). "Structural and thermal performance of steel-concrete composite floor systems: Composite slabs test. European Research project: Structural Application of Ferritic Stainless Steels (SAFSS), task 3.3", *Technical Report,* Funded by the European Community's Research Fund for Coal and Steel (RFCS).

[16] EN 1993-1-3, European Committee for Standardization (2006), "Eurocode 3. Design of steel structures. Part 1-3: General rules. Supplementary rules for cold-formed members and sheeting", Brussels, Belgium.

[17] EN 1993-1-4, European Committee for Standardization (2006) + A1 (2015), "Eurocode 3. Design of steel structures. Part 1-4: General rules. Supplementary rules for stainless steels", Brussels, Belgium.

[18] Arrayago, I., Real, E., Mirambell, E., Marimon, F. and Ferrer, M. (2017), "Experimental study on ferritic stainless steel decks in construction stage", *Submitted to Thin-Walled Structures.*

[19] ArcelorMittal (2010), "Arval Plancher Collaborant Cofraplus 60", ArcelorMittal Construction Belgium.

[20] Bonilla, J.D., Bezerra, L.M., Larrúa, R., Recarey, C. and Mirambell, E. (2015), "Study of stud shear connectors behaviour in composite beams with profiled steel sheeting", *Revista de la Construcción* **14**(3), 47-54.

[21] Chen, S., Shi, X. and Qiu, Z. (2011), "Shear bond failure in composite slabs – a detailed experimental study", *Steel and Composite Structures, An Int'l Journal*, **11**(3).

[22] Cifuentes, H. and Medina, F. (2013), "Experimental study on shear bond behavior of composite slabs according to Eurocode 4", *Journal of Constructional Steel Research*, **82**, 99-110.

[23] Ferrer, M., Marimon, F. and Crisinel, M. (2006), "Designing cold-formed steel sheets for composite slabs: an experimentally validated FEM approach to slip failure mechanics", *Thin-Walled Structures*, **44**, 1261-1271.

[24] Florides, M.M. and Cashell, K.A. (2017), "Numerical modelling of composite floor slabs subject to large deflections", *Structures*, **9**, 112-122.

[25] Kataoka, M.N., Friedrich, J.T. and El Debs, A.L.H.C. (2017), "Experimental investigation of longitudinal shear behavior for composite floor slab", *Steel and Composite Structures, An Int'l Journal*, **23**(3).

[26] Ranzi, G., Bradford, M.A., Ansourian, P., Filonov, A., Rasmussen, K.J.R., Hogan, T.J. and Uy, B. (2009), "Full-scale tests on composite steel–concrete beams with steel trapezoidal decking", *Journal of Constructional Steel Research*, **65**(7), 1490-1506.

[27] Saravanan, M., Marimuthu, V., Prabha, P., Arul, Jayachandran S. and Datta, D. (2012), "Experimental investigations on composite slabs to evaluate longitudinal shear strength", *Steel and Composite Structures, An Int'l Journal*, **13**(5).

[28] Bailey, C.G. (2003), "Large scale fire test on a composite slim-floor system". *Steel and Composite Structures, An Int'l Journal*, **3**(3).

[29] Li, G.Q, Zhang, N. and Jiang, J. (2017), "Experimental investigation on thermal and mechanical behaviour of composite floors exposed to standard fire", *Fire Safety Journal*, **89**, 63-76.

[30] Tan, K.H. and Nguyen, T.T. (2015), "Experimental and numerical evaluation of composite floor systems under fire conditions", Journal of Constructional Steel Research, 105, 86-96.

[31] Lauwens, K., Douchya, J., Fortana, M., Arrayago, I., Mirambell, E., Van Gysel, A. and Rossi, B. (2017), "Experimental study of ferritic stainless steel composite slabs", *Proceedings of the eighth European Conference on Steel and Composite Structures (EUROSTEEL)*, 1909-1918.

[32] Luu, T., Bortolotti, E., Parmentier, B., Kestermont, X., Briot, M., Grass, J.-C. (2009), "Experimental investigation of lightweight composite deck slabs", *Proceedings of the Ninth International Conference on Steel Concrete Composite and Hybrid Structures (ASCCS),* 345-350, Leeds, UK.

[33] EN1990, European Committee for Standardization (2005), "Eurocode 0. Basis of structural design", Brussels, Belgium.

[34] NF-EN1994-1-1/NA, Commission de normalisation de la construction mixte CNCMIX (2007), "Eurocode 4. Calcul des structures mixtes acier-béton. Partie 1-1: Règles générales et règles pour les bâtiments. Annexe Nationale à la NF EN 1994-1-1:2005", La Plaine Saint-Denis Cedex, France.

[35] Commission chargée de formuler des Avis Techniques (2014), “Cahier des prescriptions techniques communes aux procédés de planchers collaborants”, Marne-la-Vallée Cedex, France.

[36] Ertzibengoa, D., Matthys, S. and Taerwe, L. (2012), “Bond behaviour of flat stainless steel rebars in concrete”. *Materials and Structures*, **45**, 1639–1653.